Numerical Analysis of a Centrifugal Compressor Including a Vaneless Diffuser and a Volute

Jonas Rosemeier
Institute of Propulsion Technology, German Aerospace Center, Linder Hoehe, 51147 Cologne, Germany
jonas.rosemeier@dlr.de

Within the scope of this paper, a centrifugal compressor including a volute and a vaneless diffuser from the company Liebherr Aerospace is analyzed. The main aim of this paper is to get findings, which help to plan experimental measurements and choose meaningful positions for measurement probes. Furthermore, the flow inside the volute shall be analyzed. The focus for the investigations lies at operation point near the surge line. For the first analysis, only the impeller with a vaneless diffuser is simulated. Afterwards, the volute is taken into account and gets simulated with the impeller and the diffuser. The main findings of the study are that the instrumentation of the impeller should be focused on the leading and trailing edge of the blade. At the surge line it can be seen that the tip vortex and a region at the suction side of the blade, which is endangered of flow separation, have the biggest influence. Furthermore a region, which is endangered of flow separation, evolves at the trailing edge. The flow inside the volute is mainly dependent on the inflow angle at the inlet of the volute. The pressure distribution around the tongue of the volute could have impact on the surge and rotating stall phenomena, thus there should be measurements too.

1. Introduction

Centrifugal compressors play a substantial role in many different industrial processes, because they achieve high pressure ratios and high efficiencies at design operating point, while having a small overall size. In case of Liebherr Aerospace Toulouse SAS, centrifugal compressors are also integrated in air-conditioning systems for airplane cabins. One of these compressors is beeing investigated in the EU-project ROSSINI, which is also the framework for this study. The project ROSSINI is a cooperation between Liebherr Aerospace Toulouse, the Netherlands Aerospace Center and the German Aerospace Center, and is focused on the investigation of rotating stall and surge phenomena. During the project, the compressor will be numerically investigated at the NLR and experimental measurements will take place at the DLR in Cologne. To plan and construct the test rig, first numerical studies have to be accomplished on DLR side. These studies are object of this paper.

To get a meaningful basis for the planning of probe locations, it has to be investigated what kind of phenomena occur when the compressor works in an operating point near the surge line. Furthermore has to be researched, how the flow inside the volute behaves and if it can be seen that the volute, especially the tongue, has any influence on the location of the surge line or rather the surge itself.

2. Investigated Compressor

The compressor considered for this study, which is shown in figure 1, is a single stage centrifugal compressor which consists of an impeller, a vaneless diffuser and a volute housing. The impeller has 15 backswept, unshrouded main blades and no splitter blades. The rotation speed at the design operation point is about 46.000 rpm.

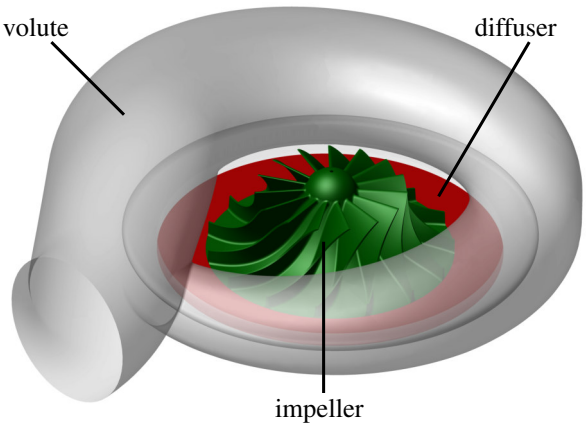

Figure 1: Overview of the investigated compressor with the vaneless diffuser and the volute

3. Numerical Setup

The simulations are performed using the flow solver TRACE in the version 9.0.411, which is developed by the Institute of Propulsion Technology in Cologne. TRACE solves the three-dimensional compressible

Reynolds-averaged Navier-Stokes equations by using an implicit finite volume method and is able to handle structured grids as well as unstructured grids. In the framework of this study, only steady calculations had been considered and in every configuration, the turbulence was modeled using the k-ω-model by Wilcox [1]. In TRACE, this model had been extended by special turbomachine-relevant modifications such as accounting for streamline curvature, effects of rotation and compressibility, and suppressing the so-called stagnation point anomaly. These additional modifications are used to make sure that TRACE is able to calculate compressor flows even in conditions close to surge [2] [3].
The boundary conditions at the inlet are the same for all simulations and include the total pressure, the total temperature, the flow angle, the turbulent intensity and the turbulent lenght scale. At the outlet, only the static pressure is set and gets changed during the simulations to reach different operation points and create the performance maps.

Two different configurations had been simulated. In the first step, only the impeller and the diffuser were simulated and in the next step, the volute housing was added and simulated together with the impeller and diffuser. In both cases, the impeller had been handled as a single passage configuration with periodic boundary conditions and the interface between the stationary parts and the rotor had been modeled by a mixingplane approach.
For the impeller, a structured grid with a CH topology was used, which had been generated using the structured multiblock mesh generator PyMesh, developed at the Institute of Propulsion Technology. The basic topology of the grid is shown in figure 2 and a schematical overview of the configuration is shown in figure 3.

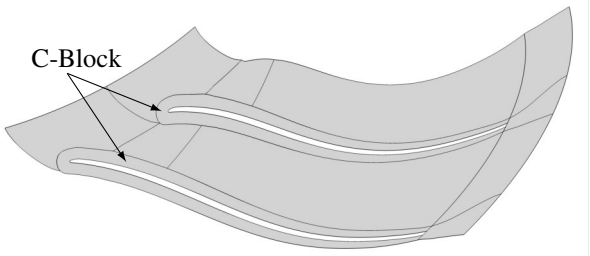

Figure 2: Topology of the impeller grid at the tip

In front of the blade, an inlet section had been added to avoid strong influences of the inlet boundary conditions. Behind the trailing edge of the blade, the vaneless diffuser with parallel walls is located. Approximately in the middle of the diffuser, the mixingplane had been added as the rotor-stator interface. For the simulations without the volute, a pinched outflow section had been added behind the diffuser to avoid an influence of the outlet boundary conditions on the diffuser outflow. This is especially important if one wants to make simulations near the surge line, where the mass flow takes low values and reversed flow can occur. Oh and Agrawal [4] and Oh et al. [5] already used a pinched section after a vaneless diffuser to avoid reversed flow at operation points of low mass flows.
For the whole grid, a low-reynolds approach was used during the simulations to calculate the boundary layers of the flow. Therefore, the dimensionless wall distance of the grid was between 0.5 and 2.5. Overall, the grid of the impeller and diffuser has about 2.7 millions cells.

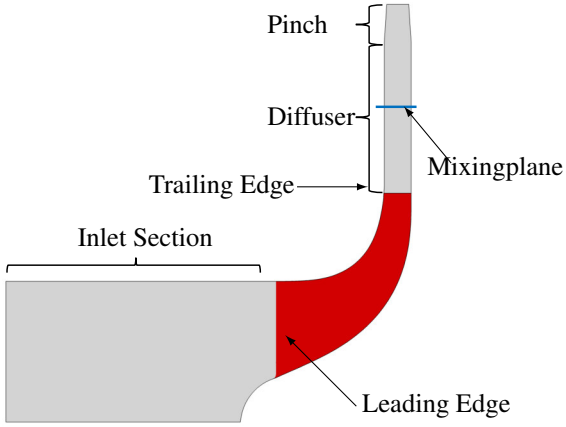

Figure 3: Schematical overview of the computational domain of the impeller

For the volute, an unstructured grid had been chosen, which was generated with the commercial mesh generator CENTAUR. In contrast to the impeller, the volute was simulated using the wall function and not the low-reynolds approach. Therefore the dimensionless wall distance is around 25 for the whole volute. In the wall regions of the grid, 10 prism layers had been added and the rest of the grid consists of tetrahedral cells. The grid hast about 2.2 millions cells.

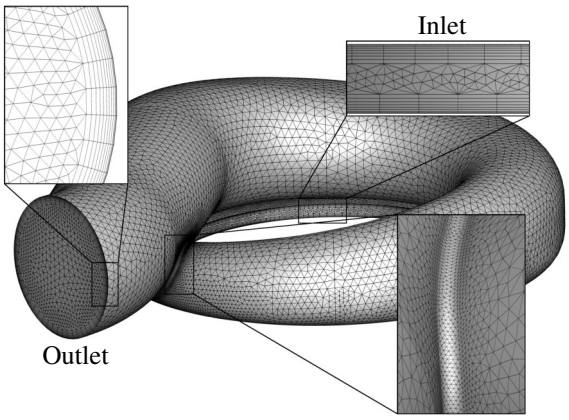

Figure 4: Overview of the unstructured grid of the volute

In figure 5 a schematic overview of the configuration with the impeller, diffuser and volute is shown. To combine the two grids, the block of the impeller grid, which is downstream of the mixingplane, had been removed and replaced by the grid of the volute.

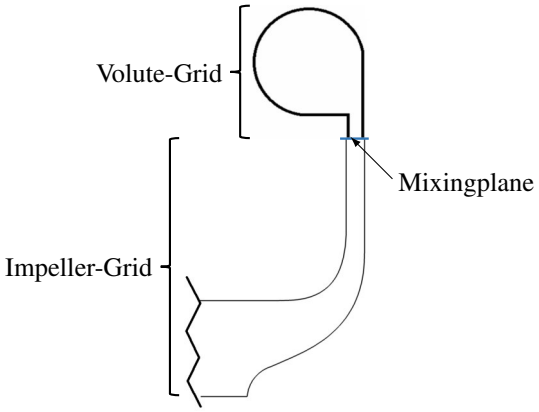

Figure 5: Schematic overview of the configuration withe impeller, diffusor and volute

4. Operating Range of the Compressor

Figures 6 and 7 show the normalized performance maps of the compressor without the volute housing. Five different speedlines had been simulated with reduced rotating speed from 28000 to 46000 rpm and the highest reduced massflow is about 0.79 kg/s. The maximum isentropic efficiency is almost the same, independently from the considered rotation speed. Near the chocke line, one can see a typical significant decrease of the isentropic efficiency whereas at the surge line there is only a small decrease. The compressor generally works under subsonic conditions, which is why no compression shocks occur inside the blade passages.

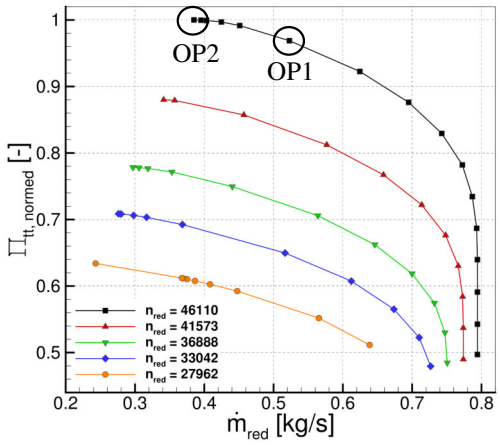

Figure 6: Normalized pressure ratio of the compressor

There are two operation points labelled inside the performance maps, which will be considered in detail below. The operation point OP1 has the highest efficiency at a rotation speed of 46000 rpm and OP2 is the last converged operation point near the surge line. At this point it has to be mentioned, that the last operation points on the left side of the speedlines represent the numerical stability limit and not the physical surge limit. Thus if hereafter the surge line is mentioned, actually the numerical stability limit is meant.

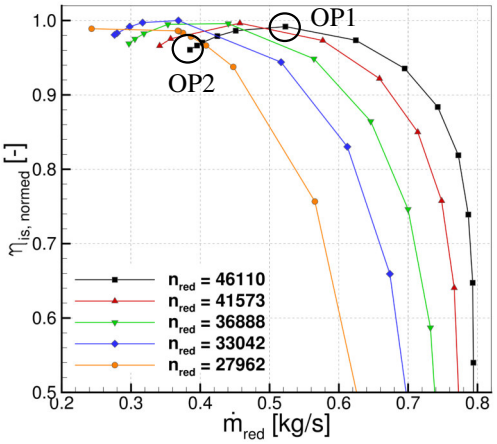

Figure 7: Normalized isentropic efficiency of the compressor

5. Phenomena at the Surge Line

To analyze the phenomena which occur at the surge line, the specific entropy distribution at the S2m-plane is considered in figure 8. The values are averaged over the scope. On the left side of the figure, one can see the operation point OP1 and on the right side the point OP2. In both operation points, the specific entropy increases slightly from the leading edge of the blade because of friction effects at the blade surfaces. At the tip region of the blade, one can see that the entropy increases downstream, triggered by the leading edge of the blade. At the operation point OP2, the increase is much higher and has a bigger spatial influence inside the blade passage. The main reason for this effect is the clearance flow respectively the clearance vortex, which is an result of the gap between the blade and the casing.

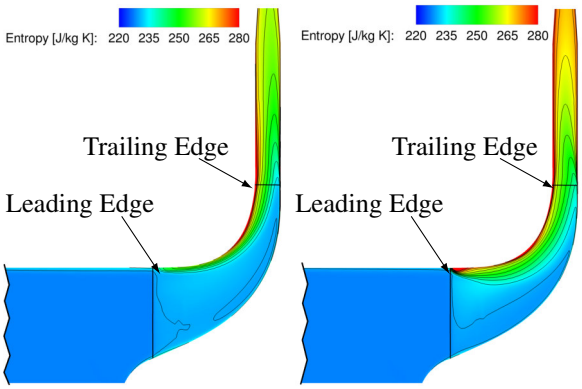

Figure 8: Entropy distribution at the S2m-plane, averaged over the scope; OP1 left, OP2 right

Another effect, which is visible at both operation points, is the generation of entropy inside the boundary

layer at the casing. At the middle and rear part of the blade, the boundary layer gets bigger because of the redirection of the fluid in the radial direction. Thereby the entropy is also increased.

To take a closer look at the loss mechanism at the leading edge of the blade, the distribution of the mach number and streamtraces are shown in figure 9. The top part of the figure shows the operation point OP1 and the lower part shows the operation point OP2 on a S1 plane at 90 % channel height. Based on the streamlines, one can see the inflow direction of the fluid. At operation point OP2 a positive incidence can be seen, whereby at the suction side of the blade a region exists which is endangered of flow separation. This leads to an area of low mach numbers on the S1 plane respectively the upper part of the blade passage.

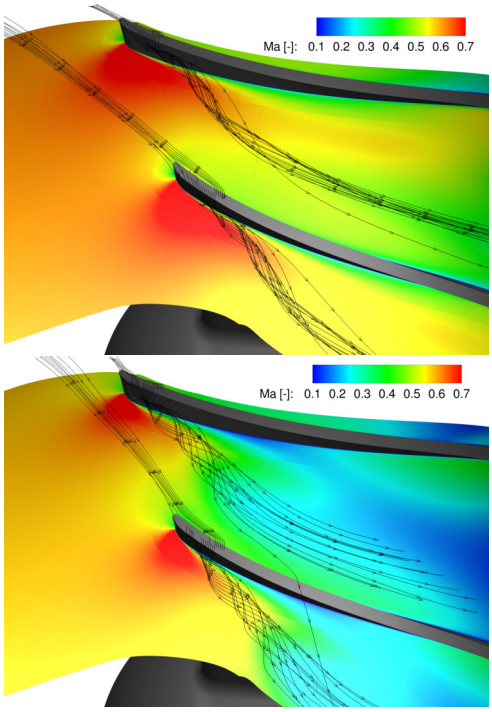

Figure 9: Distribution of the mach number and streamtraces at 90 % channel hight; OP1 at the top, OP2 at the bottom

The streamtraces also show the tip vortex, which forms from the leading edge of the blade. At operation point OP2, it is noticeable that the vortex spreads further inside the blade passage and takes more space overall compared to OP1. This also influences the velocity at the upper part of the passage and leads to regions of low mach numbers respectively low velocities in the tip region.
The danger of flow separation as well as the evolution of low velocity regions at the tip are indicators of beginning surge inside the passage, therefore the region around the leading edge should be taken in account during experimental measurements.

The flow at the rear part of the blade is shown in figure 10. It shows the rear three S3 planes in the passage, on which the distribution of the mach number can be seen and additionally streamtraces within the blade passage are displayed. At the operating point OP1, as well as OP2e, it should be noted that the speeds on the suction side of the blade are higher than on the pressure side. Furthermore, it is observed that in the middle part of the blade the areas with the greatest flow velocities in the upper part of the passage are shifted to the hub as the blade length increases. This effect results from the radial deflection of the flow, since in the front and middle area of the blade, the flow still flows mainly in the axial direction, whereas a radial outflow is present at the end of the blade. By the mass inertia the flow is thus directed towards the hub in the rear region, whereby the higher speed results. On the S3 plane in the middle of the blade, one can recognize the influence of the tip vortex when the compressor works at the operation point OP2. This is expressed by a strongly marked area of low mach numbers in the upper part of the passage, which also extends further downstream through the channel. Even at the operating point OP1, a small influence can still be found, which however is less pronounced. On the basis of the streamtraces in the figure, it is clear that the formation of wake regions in the rear part of the blade is also decisively influenced by the gap flow. The streamtraces that run through the jet regions all come out of the channel and follow the contour of the blade evenly. Through the wake regions however almost exclusively fluid flows which has previously passed through the radial gap from the adjacent blade passage. Since the gap flow and the passage flow get mixed up, the overall speed is considerably lower than in the rest of the channel. At the surge line, the velocity in the rear part of the blade at the pressure-side fillet becomes smaller and thus there exists a region which is endangered of flow separation. This can also be seen at the distribution of the wall shear stress, which is displayed on the top left part of the lower figure. The values of the shear stress become quite small, what is an indication for an almost detached flow. Against the background that this operation point is only the last numerically stable point, it is to be assumed that with a further lowering of the mass flow an so-called corner detachment occurs. This is one of the typical phenomena that occurs when a centrifugal compressor gets into surge.

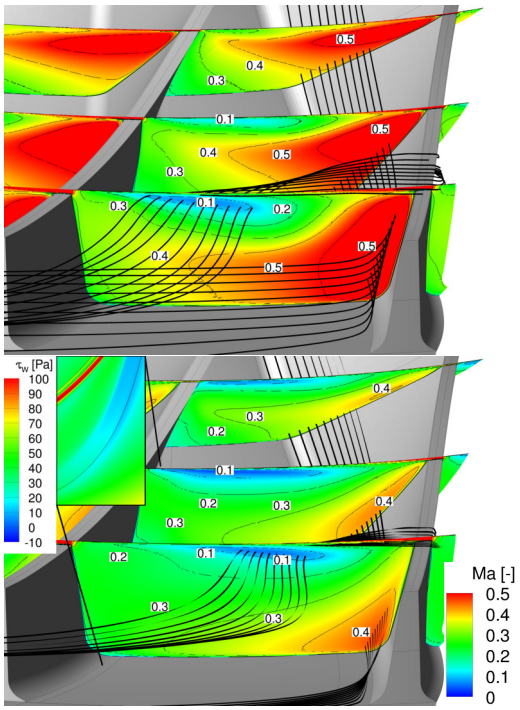

Figure 10: Distribution of the mach number at different S3-planes; OP1 at the top, OP2 at the bottom

Because of the mentioned regions which are endangered of flow separation, the rear part of the blades respectively the tailing edge of the blade should also be taken in account when it comes to the planning of measurements for the experiment.

6. Basic Flow Structure Inside the Volute

Hereinafter, all the simulations had been accomplished by using the configuration with impeller, diffuser and volute housing.

Figure 11 shows the normalized total pressure ratio in the performance map of the compressor as shown in figure 6. In addition, every speed line had now been simulated together with the volute. The course of the speed lines with the volute is basically the same as the course of speed lines without the volute. The biggest difference is that the curves with volute are shifted downwards and thus reach a smaller total pressure ratio. This is due to the fact that within the volute a total pressure loss is generated by different loss mechanisms and thus the total pressure at the outlet is lower. The position of the choke line is the same for the respective speed lines, irrespective of whether or not the volute is taken into account. In the area of the surge line, there is a difference between the curves with and without the volute at all rotation speeds. For the simulations with the volute, the surge line is reached somewhat earlier than in the case of simulations without the volute. It is to be assumed that this difference has numerical reasons, since it is not to be expected that the volute geometry has an influence on the position of the surge line. Again, there are two operation points marked, which will be considered hereinafter. OP1 is the operation point with the highest isentropic efficiency and OP2 is a point at the choke line.

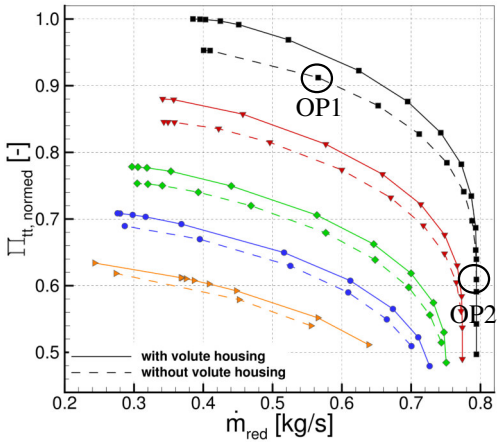

Figure 11: Comparism of the total pressure ratio with and without the volute

The basic structure of the flow within the volute is shown for OP1 in figure 12. The flow is visualized by streamtraces, which pass the whole volute from the inlet to the outlet. The flow generally consists of two circular movements which overlap and form a complex, screw-like total flow. The first movement consists of the circular flow around the rotation axis of the compressor and thus follows the overall geometry of the volute. The second movement is caused by the inflow of the fluid into the volute and the subsequent deflection into the approximately circular cross-section of the volute.

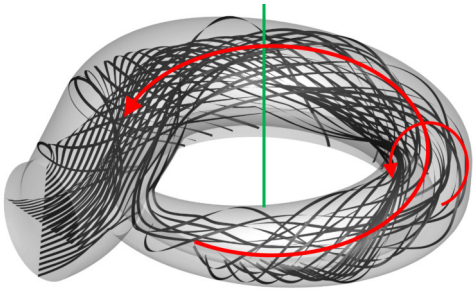

Figure 12: Basic structure of the flow inside the volute

In figure 13, a cross-section of the volute is shown for operation point OP1 on the left side and operation point OP2 on the right side. The contour plot shows the distribution of the mach number and in addition, there are projected streamtraces displayed. It can be seen, that the structure of the flow inside the volute depends on the operation point considered. At operation point OP1, two counter rotating vortices are formed, whereas at operation point OP2 only one vortex is visible. Furthermore can be seen, that at operation point OP1, there

is a big region of low velocities at the inner side of the volute, thus the inner part of the volute does not really get influenced by the flow. At the operation point OP1, the mass flow is distinctly smaller than at operation point OP2 and thus the inflow angle at the inlet is larger. This results in a more tangential inflow into the volute, which is mainly responsible for the observed behavior.

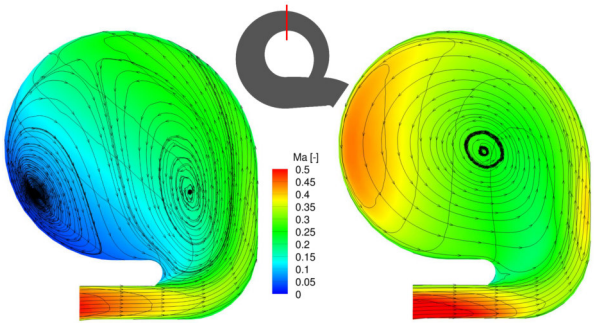

Figure 13: Evolution of vortices inside the volute, visualized on a cross-section; OP1 left, OP2 right

7. Details of the Pressure Distribution Inside the Volute

The total pressure loss which the flow is experiencing within the volute, is examined in more detail in figure 14. On the axes of the diagram the angle of incidence of the volute is plotted against the reduced mass flow and the contour plot in the background shows the pressure loss coefficient of the volute. The five curves shown represent the five speed lines, which are also shown in the performance map of figure 11. The curve on the left side being the lowest speed and the curve on the right side is the top speed. It can be seen that the pressure loss coefficient, and thus the total pressure loss, is greatest when the inflow angle is small. It can also be seen that the pressure loss coefficient becomes greater when the inflow angle assumes very large values, thus there is a range between 48 and 58 ° in which the pressure loss coefficient is the smallest. This is the operating range on which the geometry of the volute was designed and optimized. If a certain inflow angle is considered and only the mass flow gets changed, it is noted that the pressure loss coefficient is almost independent of the mass flow and is almost exclusively dependent on the inflow angle.

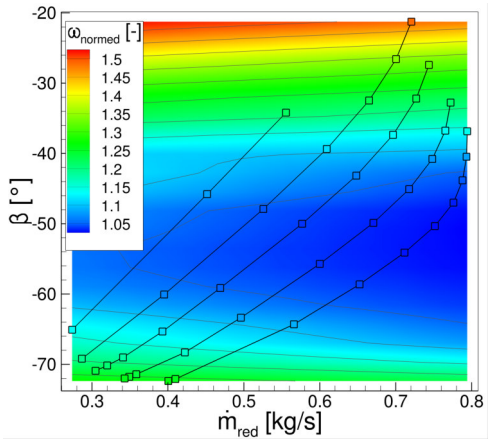

Figure 14: Dependency of the pressure loss coefficient from the incident angle of the volute and the mass flow

The pressure profile over the entire through-flow cross-section of the volute is shown at different levels in figure 15 for OP1. It can be seen here that the static pressure in the diffuser or parallel-walled entry region of the volute continues to rise. By deflecting the flow from the inlet region into the upper round body of the volute and the associated centrifugal force, the static pressure increases at the outer wall of the volute and reaches the maximum values at the lower part of the outer wall, since here the deflection is greatest. By the deflection of the flow and the continuous enlargement of the cross-sectional area, the flow is further retarded, which also results in a conversion of the kinetic energy to static pressure.

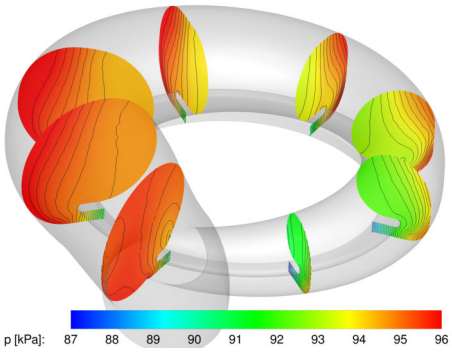

Figure 15: Pressure distribution on different cross-sections of the volute

At the inner wall of the volute the pressure is basically lower than at the outer wall, since the flow follows a circular path and the centrifugal force is forced outwards. At the outlet of the volute, or the largest area shown, the static pressure has clearly increased in comparison to the smallest cross-sectional area. The entire volute therefore also acts as a diffuser and additionally contributes to the transformation of the kinetic energy of the flow in static pressure. The cross-sectional extension along the volute is large enough that the

flow is further retarded although additional fluid enters the volute continuously at each location of the inlet.

In figure 16, the distribution of the static pressure at the entrance into the volute for the operating point OP1 is shown. The illustrated plane is at 50 % of the height of the diffuser, as shown in the figure at the top right. In principle, it can be seen that the static pressure at the inlet of the volute is the lowest and a continuous increase with increasing radius is present. This increase in pressure results from the deceleration of the flow in the inlet region of the volute, or the outlet region of the diffuser. Also in the entrance region, the cross-section increases further and thus the speeds decrease. In the region behind the tongue, the lowest pressures are present, and downstream, the pressures are continuously increased. The reason for the low pressure in the tongue region lies in the larger velocities, which on the one hand results from the fact that the cross section of the volute is the smallest shortly after the tongue, and is continuously increased along the volute. On the other hand, a part of the fluid flows from the rear, thicker area of the volute likewise again through the area of the smallest cross-section, which increases the mass flow at this point.

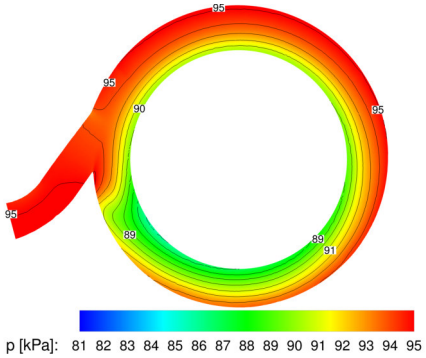

Figure 16: Pressure distribution at the inlet section of the volute

The flow respectively the flow separation in the region of the volute tongue is shown in figure 17 in more detail. Here, the distribution of the mach numbers together with streamtraces for the operating point OP1 (left) and the operating point OP2 (right) is displayed. Basically, it can be seen that parts of the flow from the wide part of the volute do not leave directly through the exit of the volute, but enter the narrow part and pass the volute once more. The main criterion for whether the fluid emerges from the volute or once again enters the narrow part, is the ratio of the flow velocity to the pressure gradient between the broad part and the narrow part. Already in figure 16 it was shown that the static pressure in the narrow part of the volute, right behind the tongue is lowest and thus a pressure gradient from the wide part of the volute to the narrow part exists. Figure 17 shows that at the operating point OP1 a larger proportion of the flow is again deflected into the narrow part of the volute since the flow velocities or the mass inertia are lower than on the choke line and thus the pressure gradient has a bigger influence on the flow. At operation point OP2 a small fraction of the flow is also deflected by the pressure gradient, but due to the greater mass inertia, this is significantly less. A further influencing factor for the deflection of the flow is the inflow angle at the inlet of the volute. In the figure, it can be seen clearly that the flow at choke limit, due to the more radial inflow, rather flows past the tongue and thus the required deflection in order to flow into the narrow region is greater than in the operating point OP1. Referring to figure 14, it can be seen why the pressure loss increases if the inflow angle takes high values. Because at large inflow angles a larger part of the flow enters the volute a second time and the pressure loss becomes greater due to friction effects. Furthermore, it is clear from figure 17 that the volute is optimized for certain inflow angles, since only in certain areas there is an optimal flow around the tongue guaranteed.

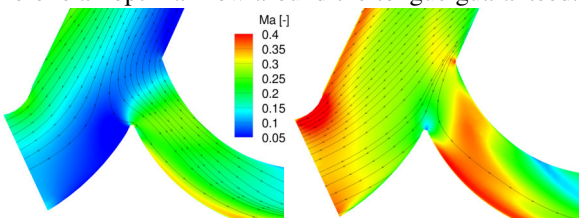

Figure 17: Distribution of the mach number around the tongue of the volute

The formation of surge and rotating stall is strongly dependent of the pressure at the outlet of the impeller The figures 17 and 16 show that there are pressure differences around the tongue of the volute and thus the pressure is not equal around the scope of the impeller, respectively the volute. Against this background, the tongue could have a clear influence on the surge and rotating stall of the compressor, thus the region around the tongue should be taken into account while the experimental measurements. Figure 18 shows the configuration of the whole compressor, including the volute. By taking a closer look at the geometry, it shows that the region, which is marked in the figure, is the only possible location to get access on the diffuser and the interesting region around the tongue with optical measurement techniques. Because of this facts, optical measurements will be carried out at this location.

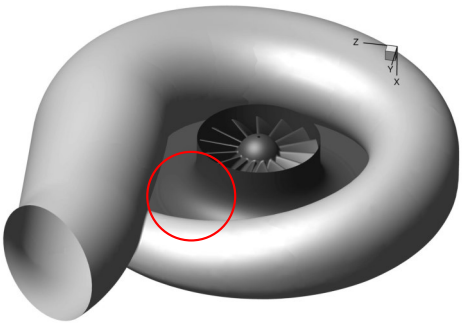

Figure 18: Overview of the compressor with marked region for optical measurements

8. Conclusions

To get a meaningful basis for the planning of a future measurement campaign in the framework of the EU-project ROSSINI, a centrifugal compressor with a vaneless diffuser and a volute housing had been numerically analyzed. The main targets of this study were to get an overall impression how the compressor behaves, what kind of effects occur near the surge line, how the flow inside the volute behaves and if there are any indications for an influence of the volute tongue on the surge and rotating stall phenomena. The results of the study can be summarized as follows.

1. At the leading edge of the blade, the tip vortex gets bigger and has a greater influence on the flow, when the compressor works in operation points at the surge line. By that, the result is a large region of low velocities at the tip.
   At the suction side of the blade, a region which is endangered of flow separation, occurs as a result of a positiv incidence while working at the surge line.
2. At operation points at the surge line, it is noticeable that at the rear part of the blade, a region occurs at the pressure-side fillet, which is endangered of flow separation.
3. During the future measurements, the main attention will be on the region at the leading edge and at the trailing edge, thus there will be optical measurement probes installed. This results from the last two conclusions.
4. In the case of large mass flows and small inflow angles, a uniform vortex is formed on the cross sections of the volute. In the case of small mass flows and large inlet angles, on the other hand, there is a tendency to form two counter rotating vortices on the cross sections.
5. The total pressure loss inside the volute is almost exclusively dependent on the inflow angle at the inlet of the volute. An optimal inflow angle approximately lies between 48 and 58°. Higher and lower angles result in a higher total pressure loss, whereby the mass flow has almost no influence on the losses. The static pressure increases inside the volute, thus the volute also acts as diffuser.
6. Around the tongue of the volute, considerable pressure differences can bee seen. These differences could trigger surge or rotating stall effects and should be taken into account during the measurements. Optical measurement probes will be installed near the tongue.

Nomenclature

$\dot{m}_{red}$	reduced mass flow
$\Pi_{tt,normed}$	normalized total pressure ratio
$\eta_{is,normed}$	normalized isentropic efficiency
Ma	mach number
β	inflow angle at the inlet of the volute
ω_{normed}	normalized total pressure loss coefficient
p	static pressure

Acknowledgment

This paper has been prepared in the framework of a project that has received funding from the *European Union's Horizon 2020 research and innovation programme* under grant agreement No 717081

References

[1] David C. Wilcox. Reassessment of the scale-determining equation for advanced turbulence models. *AIAA Journal*, (26):1299–1310, 1988.

[2] Thomas Röber, Dragan Kožulović, Edmund Kügeler, and Dirk Nürnberger. *Appropriate Turbulence Modelling for Turbomachinery Flows using a Two-Equation Turbulence Model*, pages 446–454. Springer Berlin Heidelberg, Berlin, Heidelberg, 2006.

[3] Franke M.,Röber T.,Kügeler E.,Ashcroft G. Turbulence treatment in steady and unsteady turbomachinery flows. *In Proceedings Fifth European Conference on*, 2010.

[4] Giri L. Oh, JongSik und Agrawal. *Numerical Investigation of Low Solidity Vaned Diffuser Performance in a High-Pressure Centrifugal Compressor: Part I — Influence of Vane Solidity*. 2007.

[5] Charles W. und Agrawal Giri L. Oh, JongSik und Buckley. *Numerical Investigation of Low Solidity Vaned Diffuser Performance in a High-Pressure Centrifugal Compressor: Part II— Influence of Vane Stagger*. 2008.